Available online at www.sciencedirect.com
SCIENCE DIRECT
Vision Research 46 (2006) 2645–2658
Vision Research
www.elsevier.com/locate/visres

Meta- and paracontrast reveal differences between contour- and brightness-processing mechanisms

Bruno G. Breitmeyer [a,c,*], Hulusi Kafalıgönül [b], Haluk Öğmen [b,c], Lynn Mardon [d,1], Steven Todd [d,1], Ralph Ziegler [a]

[a] Department of Psychology, University of Houston, Houston, TX 77204-5022, USA
[b] Department of Electrical and Computer Engineering, University of Houston, Houston, TX, USA
[c] Center for Neuro-Engineering and Cognitive Science, University of Houston, Houston, TX, USA
[d] Department of Philosophy, University of Houston, Houston, TX, USA

Received 18 February 2005; received in revised form 4 October 2005

Abstract

We investigated meta- and paracontrast masking using tasks requiring observers to judge the surface brightness or else the contours of target stimuli. The contour task revealed strongest metacontrast at SOAs shorter than those obtained for the brightness task. Paracontrast revealed related temporal differences between the tasks. Additionally, the paracontrast results support the existence not only of prolonged inhibitory effects but also of facilitatory effects. The combined results comport with the existence of cortical mechanisms for: (i) fast contour processing, (ii) slow surface-brightness processing, (iii) prolonged inhibition, and (iv) facilitation.
© 2005 Elsevier Ltd. All rights reserved.

Keywords: Contour processing; Brightness processing; Temporal properties; Visibility suppression; Visibility enhancement; Surface-contrast processing

1. Introduction

Metacontrast and paracontrast are types of visual masking in which the visibility of one briefly flashed stimulus, called the target, can be suppressed by a briefly flashed second stimulus, called the mask, which precedes or follows the target by varying onset asynchronies (SOAs). Performance in visual masking studies depends on the criterion content used by an observer (Bernstein, Fisicaro, & Fox, 1976; Hernandez & Lefton, 1977; Hofer, Walder, & Groner, 1989; Kahneman, 1968; Petry, 1978; Stoper & Mansfield, 1978; Ventura, 1980). Criterion content is determined by the task requirements and refers to the stimulus dimension along which an observer is asked to make his or her perceptual judgment about the target. For instance, if the observer is asked to respond to the *mere occurrence* or *location* of a target stimulus, one often obtains no masking effect (Bernstein, Amundson, & Schurman, 1973; Fehrer & Biederman, 1962; Fehrer & Raab, 1962; Harrison & Fox, 1966; Öğmen, Breitmeyer, & Melvin, 2003; Vorberg, Mattler, Heinecke, Schmidt, & Schwarzbach, 2003, 2004). However, if (s)he is asked to respond on the basis of perceived *brightness* or *form*, one does obtain target suppression that varies as a U-shaped function with SOA (Alpern, 1953; Breitmeyer, Love, & Wepman, 1974; Cavonius & Reeves, 1983; Enns & Di Lollo, 1997; Kolers & Rosner, 1960; Öğmen et al., 2003; Stober, Brussel, & Komoda, 1978; Tata, 2002; Weisstein, 1972). Even here the specific shape and temporal characteristic of the U-shaped function should depend on which of the two criterion contents, brightness or form, is used. We base this hypothesis on the following considerations.

According to current theorical modeling (Grossberg, 1994; Grossberg & Mingolla, 1985), supported by neurophysiological findings (DeYoe & Van Essen, 1988; Lamme,

* Corresponding author. Tel.: +1 713 743 8570; fax: +1 713 743 8588.
E-mail address: brunob@uh.edu (B.G. Breitmeyer).
[1] Present address: Department of Philosophy, University of Connecticut, CT, USA.

0042-6989/$ - see front matter © 2005 Elsevier Ltd. All rights reserved.
doi:10.1016/j.visres.2005.10.020

Rodriguez-Rodriguez, & Spekreijse, 1999; Xiao, Wang, & Felleman, 2003), a cortical Boundary-Contour-System (BCS) and a cortical Feature-Contour-System (FCS) process a visual object's contour and surface properties, respectively. Moreover, the BCS and FCS correspond to the parvocellular, P-interblob and P-blob streams in the cortical object object-processing pathway (Grossberg, 1994). Francis (1997) recently applied the BCS to modeling of various metacontrast and other spatiotemporal phenomena (Francis, 1996a, 1996b). As noted by Breitmeyer and Ogmen (2000), a more complete model would require incorporation of the FCS. Along with others (Arrington, 1994; Elder & Zucker, 1998; Lamme et al., 1999), we propose that the cortical processing of surface and contour properties of a stimulus correspond to activities in a *slow* FCS and a *faster* BCS. The purpose of the present study is to use not only metacontrast but also paracontrast masking to investigate the distinctive temporal response properties of the cortical surface- and contour-processing streams.

2. Metacontrast

Differences between metacontrast masking of contour and surface properties have been investigated previously by Petry (1978) and Stober et al. (1978). In Stober et al.'s (1978) study, observers were required to make subjective magnitude estimates of the masked target's brightness and of its contour clarity or edge definition relative to an unmasked target stimulus. Stober et al. (1978) reported a negative correlation or dissociation between estimates of target brightness and contour clarity at short SOAs and a positive association between the two estimates at longer SOAs. Similarly Petry (1978), required her observers to estimate the brightness at the center and at the edge of a target disk. Brightness estimations at the center of the target disk were consistently larger (thus indicating less masking) than estimations at the edge of the disk. However, in both studies inter-observer differences of the temporal waveforms and optimal SOAs for surface and edge masking make it difficult to draw firm conclusions regarding the temporal response properties of surface and contour processing.

We employ a model-driven approach to make specific predictions about differences between the time courses of the metacontrast masking of surface and contour properties of the target. For a theoretical standpoint, we adopt the RECOD model of masking recently proposed by Öğmen (1993) and Öğmen et al. (2003). This model adopts the sustained-transient channel approach originally proposed by Breitmeyer and Ganz (1976) and updates it by relating the sustained- and transient-channel activities to activities in the parvocellular or P and magnocellular or M pathways, respectively. It is assumed in this model that besides inhibitory interactions within each of the pathways (*intra*channel inhibition), inhibitory interactions also exist between the fast M and the slower P pathways (*inter*channel inhibition). In the model, the latter interchannel inhibitory interactions are primarily responsible for metacontrast. Here, the fast M activity of the mask stimulus can inhibit the target's slower P contour-processing activity as well as the target's still slower P surface-processing activity. Consequently one should obtain optimal metacontrast suppression of the contour and surface-contrast at shorter and longer SOAs, respectively.

3. Methods

3.1. Observers

Four observers, including the authors BB (57-yr old male) and LM (47-yr old female), were used in this study. The other two volunteer observers, a 23-yr and a 22-yr old female, were practiced psychophysical observers but naïve as to the purposes of the experiment. All observers had normal or corrected-to-normal vision.

3.2. Stimuli and apparatus

The experiment was performed in a dark room. The stimuli were displayed at 100 Hz frame rate on a Sony Trinitron color monitor. Stimulus presentation and response recording were controlled by a Visual Stimulus Generator (VSG2/5) card manufactured by Cambridge Research Systems. Fig. 1 illustrates the stimulus configuration used in the brightness judgment and in the contour discrimination tasks. The fixation mark consisted of a small (0.4 deg × 0.4 deg) dark (0.5 cd/m^2) cross in the center of the screen. In the brightness judgment task, the stimuli consisted of a ring mask which spatially surrounded the right disk and a two-disk display. The right disk served as the target and the left disk as the comparison stimulus. The target and comparison disks had a diameter of 0.85 deg and the mask ring had inner and outer diameters of 0.85 and 1.27 deg, respectively. The right target–mask sequence and the left comparison disk were centered 1.4 deg above fixation and 1.6 deg to the right and left of fixation, respectively. The luminance of the target disk was 30.5 cd/m^2; that of the mask disk could be 56, 30.5, or 0.5 cd/m^2. Against a uniform background luminance of 95 cd/m^2, these three values corresponded to contrasts of 25, 51, and 99%. The mask-to-target contrast ratio (M/T ratio) thus could be (approximately) 0.5, 1.0, or 2.0. The luminance of the comparison disk could be adjusted adaptively by the observer. The mask and the target were presented for 10 ms each. In the contour identification task, the same mask ring was used. However, the target could consist of a complete disk, a disk with a 0.37-deg wide upper contour deletion (shown in Fig. 1) or a disk with the lower contour deletion of the same size. The target (followed by the surrounding mask) could be shown at the upper left or upper right stimulus locations described above. For both tasks the following target–mask SOAs were used: 0, 10, 20, 40, 60, 80,

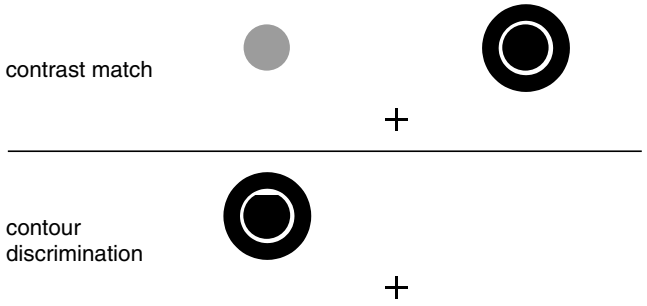

Fig. 1. Schematic diagram of target disks and mask rings used in the brightness match procedure (upper panel) and in the contour discrimination procedure (lower panel). Plus signs designate the fixation cross. See text for further details.

110,140, 170, 200, 350, and 500 ms. Moreover, a no-mask (target only) condition was also used in order to obtain baseline performance for both the brightness match and the contour identification tasks.

3.3. Procedure

For the brightness matching task, an experimental session consisted of three blocks of trials, one for each of the three M/T contrast ratios. The order of contrast ratios was counterbalanced across three sessions. Within each block, the order of metacontrast SOAs, ranging from 0 to 500 ms and including the baseline, no-mask condition, was randomly determined. At each SOA the luminance of the match stimulus changed according to the subject's response. Initially the comparison disk was either clearly brighter or darker than the target disk. On any trial, the observer's task was to report, by pressing one of two response buttons, which of the two disks, the target or the comparison, appeared brighter. The point of subjective equality (PSE) was estimated by a 1-up 1-down staircase procedure. If the comparison disk appeared darker than the target disk on a trial, its luminance was increased stepwise on the next trial. Conversely, if the comparison disk appeared brighter than the target disk, its luminance was decreased on the next trial by the same amount. For the initial three reversals the step sizes were in units of 10 (out of a total of 255) grey levels, corresponding to a luminance change of 2.4 cd/m^2. After the third reversal, step sizes were in units of one grey level, corresponding to a luminance change of 0.24 cd/m^2. At this step size luminance reversals of the comparison disk were recorded, and the PSE of the target disk for a given SOA was calculated as the average of the last six luminance reversals of the comparison disk. As a result, three average brightness-match values were obtained for each observer at each combination of SOA and M/T contrast ratio, from which the observer's overall mean was calculated. These served as the data for off-line statistical analysis. For the contour identification task, the procedure was the same except for the following changes. At each SOA, the location of the target–mask sequence was randomized across 30 trials, with half of the trials devoted to the upper left location, the remaining half to the upper right location. Of the 30 trials, 10 were devoted to each of the three possible target contours. Order of target contours was randomized across the 30 trials. After each trial the observers were required to indicate, by pressing one of three keys, which of the three targets was presented. If the observers did not see the target, they were asked to guess. Here an observer's proportion of correct contour identifications was based on a total of 90 trials at each combination of SOA and M/T contrast ratio. These proportions served as data again for off-line statistical analysis.

3.4. Results

The results are based on the log of normalized target visibilities. In the brightness match task, target brightness visibilities at each SOA were normalized relative to the target's brightness match obtained in the baseline, no-mask condition. In the contour identification task, target contour visibilities were normalized relative to the range of correct-response proportions obtained at the upper limit in the baseline, no-mask condition and at the lower limit (when the target was invisible) by a guessing probability of .33. These normalized visibilities averaged across the four subjects are shown at each M/T contrast ratio in Fig. 2A. Both brightness match and contour identification tasks yield typical U-shaped metacontrast functions, with target visibilities being high at an SOA of 0 ms, dropping to a minimum at intermediate SOAs, and then increasing to a high value at an SOA of 140 ms, after which the visibilities attain a constant, asymptotic value. For that reason, a three-way (Task × M/T Contrast Ratio × SOA) within-subject ANOVA was limited to the eight SOAs ranging from 0 to 140 ms. While the overall effect of task and contrast were not significant [$F(1,3) = 0.24$, $p > .65$; $F(2,6) = 3.10$, $p > .11$], the results of SOA were significant [$F(7,21) = 11.21$, $p < .001$]. Both tasks yielded a U-shaped masking function at SOAs ranging from 0 to 140 ms. Correspondingly a within-subjects analysis of contrasts yielded a significant quadratic trend [$F(1,3) = 20.06$, $p < .025$]. In addition the interaction between task and SOA also was significant [$F(7,21) = 3.21$, $p < .02$]. The interaction, apparent from inspection of Fig. 2A, reveals that the SOA at which optimal suppression of visibility occurred was consistently lower in the contour identification task than in the brightness matching task. Fig. 2B (see dashed arrows) amplifies this finding by showing the results for the two tasks averaged across contrast ratios. The significance of these findings will be discussed below in Section 5.

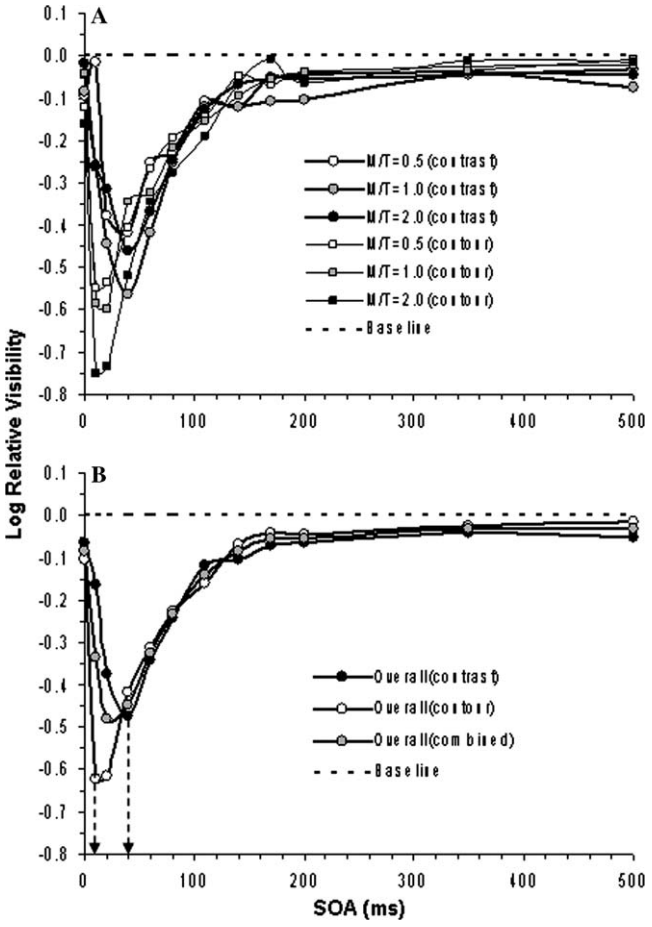

Fig. 2. (A) Log relative visibility of the target during metacontrast as a function of SOA, shown separately for the brightness-match and the contour-identification tasks at each of three different mask-to-target (M/T) contrast ratios, as indicated in the inset. (B) Log relative visibility of the target during metacontrast as a function of SOA, shown for the brightness-match and the contour-identification tasks averaged across the three (M/T) contrast ratios, as indicated in the inset. Dashed arrows indicate SOA at which maximum suppression of visibilities occur.

4. Paracontrast

Here we again adopt the RECOD model of masking (Öğmen, 1993; Öğmen et al., 2003). In the model, intrachannel inhibitory interactions are primarily responsible for paracontrast effects. Like the effects of metacontrast, those of paracontrast also depend on task requirements and thus on criterion contents. For instance, Kaitz, Moniz, and Nesher (1985), who required their observers to rate the overall visibility of the target, reported two paracontrast masking maxima; one occurring near an SOA of 0 ms, the other at SOAs falling between −100 and −200 ms. Since Kaitz et al. (1985) did not specify what

aspect of the target to report, it is possible that the two maxima may have resulted because observers correspondingly adopted two criterion contents; one based on contour clarity and the other on perceived brightness. This is a reasonable hypothesis in view of the following. Kolers and Rosner (1960), using a form identification task, report optimal paracontrast suppression at relatively short SOAs of −40 ms (mask precedes the target). On the other hand, several investigators (Cavonius & Reeves, 1983; Foster & Mason, 1977; Öğmen et al., 2003) who employed a brightness perception task obtained optimal paracontrast at longer SOAs ranging from −100 to −200 ms. To more firmly test this hypothesis, we compared paracontrast masking in a contour identification task to paracontrast in a brightness matching task. The methods of procedure were identical to those used in the metacontrast experiment, except that the target–mask SOAs now assumed the following values: 0, −10, −20, −40, −60, −80, −110, −140, −170, −200, −350, −500, and −750 ms.

4.1. Results

The results again are based on normalized target visibilities as described above. These normalized visibilities averaged across the four subjects are shown at each M/T contrast ratio in Fig. 3A. Both brightness match and contour identification tasks tended to yield paracontrast functions with somewhat complicated nonmonotonicities. In particular, the functions show not only suppression of visibility over intermediate ranges of SOA values but also some counteracting facilitation of visibility over shorter ranges. These trends can be unraveled by taking a closer look at the results of the three-way (Task × M/T Contrast Ratio × SOA) ANOVA. From inspection of Fig. 3 it appears that visibility is overall more strongly suppressed for the contour identification than the brightness matching task, although the main effect of task approached, but did not attain, significance [$F(1,3) = 6.74$, $p = .08$]. The main effect of contrast was significant [$F(2,6) = 5.23$, $p < .05$]. The overall target visibilities were −0.064, −0.047, and −0.064 for the M/T contrast ratios of 0.5, 1.0, and 2.0, respectively. The effect of M/T contrast ratio was thus nonmonotonic, as reflected in an analysis of within-subject contrasts yielding a significant quadratic trend of M/T contrast ratio [$F(1,3) = 15.20$, $p < .03$]. This nonmonotonic effect of M/T contrast on target visibilities appears somewhat paradoxical, since one would expect suppression of target visibility to monotonically increase with the mask contrast. However, since facilitation is observed in paracontrast but not in metacontrast (compare Figs. 2 and 3), it appears that in paracontrast the contrast-dependent suppression effect was counteracted by the facilitation effect that also depended on M/T contrast ratio. The main effect of SOA also was significant [$F(12,36) = 2.97$, $p < .006$]. This can be seen in Fig. 3B by inspecting the curve labeled 'Overall(combined)', which displays target visibilities averaged across contrasts and tasks. Relative to the baseline

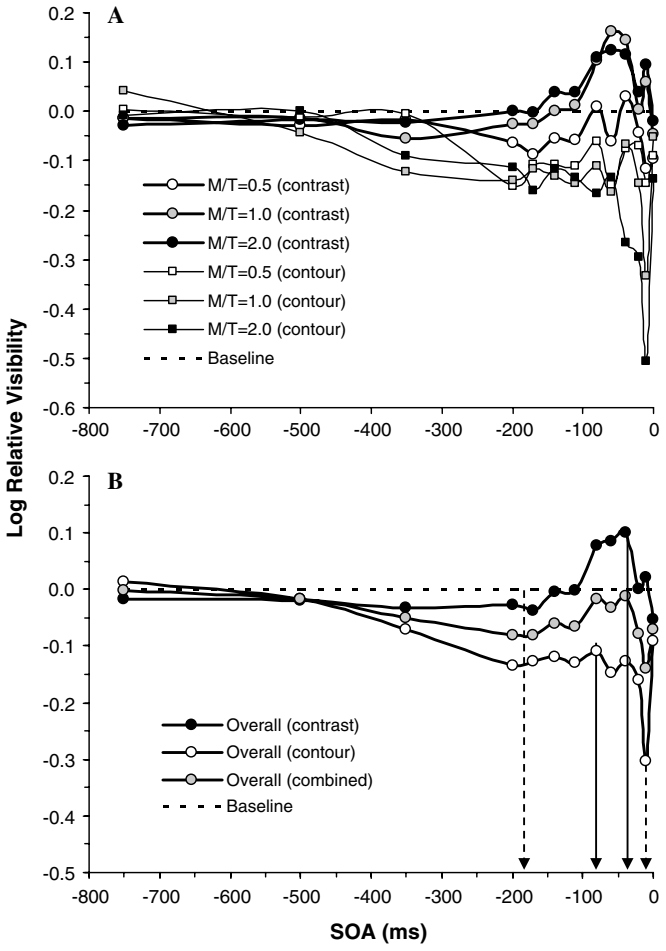

Fig. 3. (A) Log relative visibility of the target during paracontrast as a function of SOA shown separately for the brightness-match and the contour-identification tasks at each of three different mask-to-target (M/T) contrast ratios, as indicated in the inset. (B) Log relative visibility of the target during paracontrast as a function of SOA shown for the brightness-match and the contour-identification tasks averaged across the three (M/T) contrast ratios, as indicated in the inset. Dashed arrows indicate SOA at which local maxima of the suppression of visibilities occur. Dotted arrows indicate SOA at which local maxima of facilitation of visibilities occur.

visibility, variations of SOA generally produced a decrease of target visibility, that varied nonmonotonically, with local minima at SOAs at −170 and −10 ms and a local maximum at an SOA of −40 ms. This nonmonotonicity was reflected in a within-subjects analysis of contrasts that yielded a significant cubic effect [$F(1,3) = 23.48$, $p < .02$].

Regarding two-way interactions, task and M/T contrast ratio interacted significantly [$F(2,6) = 9.07$, $p < .015$], as did task and SOA [$F(12,36) = 2.21$, $p < .035$]. The former interaction indicates that increases of the M/T contrast ratio had divergent effects on target brightness and contour visibilities; i.e., the *enhancement effect increased* in the brightness matching task whereas the *suppression effect increased* in the contour identification task. For the M/T contrast ratios of 0.5, 1.0, and 2.0, the overall target visibilities in the brightness matching task showed nonmonotonic

trend with values of −0.046, 0.024, and 0.036, respectively; whereas in the contour identification task they showed a decreasing trend with values of −0.083, −0.118, and −0.163, respectively. The latter, Task × SOA interaction indicates that as SOAs approached 0 ms, the target brightness visibilities generally tended to diverge increasingly from the target contour visibilities. This can be seen by comparing the differences between the two corresponding curves in Fig. 3B as SOA proceeds from −750 to 0 ms. The interaction between M/T contrast ratio and SOA approached significance [$F(24,72) = 1.60$, $p = .065$]. It appears that while increases of M/T contrast ratios tended to yield increasing suppression at SOAs ranging from −750 to −170 ms and an SOA of −10 ms, they yielded increases of facilitation at the intermediate SOAs ranging from −140 to −20 ms. Finally, the three-way interaction among task, M/T contrast ratio and SOA also was significant [$F(24,72) = 2.80$, $p = .001$]. This interaction indicates that the above mentioned divergence of M/T contrast ratio effects with respect to task becomes more pronounced as SOA approaches 0.

Also shown in Fig. 3B are local maxima and minima in the masking functions obtained for the brightness matching and the contour identification tasks. A minimum of target brightness and contour visibilities (see left most dashed arrow) is obtained at an SOA between −170 and −200 ms. Beyond that value the target brightness visibility increases dramatically, attaining an enhanced visibility (relative to baseline) of 0.1 at an SOA of −40 ms (see right most dotted arrow), and then decreases as SOA approaches 0 ms. In comparison, target contour visibility is at an absolute minimum at an SOA of −10 ms (see right most dashed arrow), where its brightness visibility is still at baseline. Between the minima at −170 and −10 ms, there does not appear to be a clear enhancement effect, although a "local maximum" exists at an SOA of −80 ms (see left most solid arrow).

5. Discussion

Although the variation of target visibilities with SOA were more complex for paracontrast than for metacontrast, the results overall indicate distinctions and dissociations between a target's contour and brightness visibilities during both masking procedures. Below, we will present evidence that these distinctions parallel activities in distinct cortical contour and surface-brightness processing mechanisms. We turn first to a more detailed discussion of this dissociation obtained with metacontrast masking.

5.1. Metacontrast

The main finding of the metacontrast experiment was the different SOA values at which optimal suppression of the target's brightness and contour occurred. Somewhat related findings have been reported by Stober et al. (1978). Stober et al. reported a negative correlation or dissociation between estimates of target brightness and target contour clarity at short SOAs and a positive association between the two estimates at longer SOAs. These results resemble ours in that our metacontrast functions developed in parallel for longer SOAs ranging from 60 to 500 ms, but attained optimal suppression of contour and brightness visibilities at distinct values of 10–20 and 40 ms, respectively (see Fig. 2B). We take this as evidence for: (i) the existence of separate cortical mechanisms responsible for processing of a visual object's contours and its surface brightness, and (ii) related differences between their respective temporal response characteristics, with the contour mechanism being faster than the surface-contrast mechanism. The first conclusion is supported not only by extant psychophysical results (Arrington, 1994; Elder & Zucker, 1998; Paradiso & Nakayama, 1991; Stoper & Mansfield, 1978) but also by neurophysiological findings (DeYoe & Van Essen, 1988; Lamme et al., 1999; Xiao et al., 2003) indicating that activities in cortical P-interblob and P-blob pathways are associated with the processing of form and surface properties, respectively (Grossberg, 1994). The second conclusion is consistent again with prior psychophysical results (Arrington, 1994; Elder & Zucker, 1998) and with neurophysiological results showing that contours of visual stimuli are processed faster than are its surface properties (Lamme et al., 1999; Lee, Mumford, & Schiller, 1995). In terms of the dual-channel RECOD model of masking (Öğmen, 1993; Öğmen et al., 2003), these results can be accommodated, as schematized in Fig. 4, by unlumping the P-pathway driven post-retinal network into two networks, one processing contour and a second processing surface-brightness information. In RECOD, the input is processed first by short-latency transient and longer-latency sustained retinal ganglion cells. These cells give rise to parallel magnocellular (M) and parvocellular (P) pathways projecting to post-retinal areas. Post-retinal areas that receive dominant M and P inputs form the psychophysically identified transient and sustained channels, respectively. One can identify two types of inhibitory connections that play a major role in masking: Inhibition within each channel (intra-channel inhibition) and reciprocal inhibition between the sustained and transient channels (inter-channel inhibition) (Breitmeyer & Ganz, 1976). According to the model, transient-on-sustained *inter*-channel inhibition is the main mechanism of metacontrast. As depicted in Fig. 5, each briefly flashed stimulus produces a fast transient (M) activation, a slower sustained (P) contour process and in addition a still slower sustained (P) surface/brightness process. Each of the latter activities produced by the target can be suppressed (see dashed vertical arrow) by the fast transient activity of the mask. Although only showing the suppression of the target's contour process, it is evident from Fig. 5 that the model correctly predicts that the SOA of optimal suppression should be shorter for contour visibility than for brightness visibility.

A complete description of the model is given in Appendix A. Fig. 6 shows simulations of the model (bottom pan-

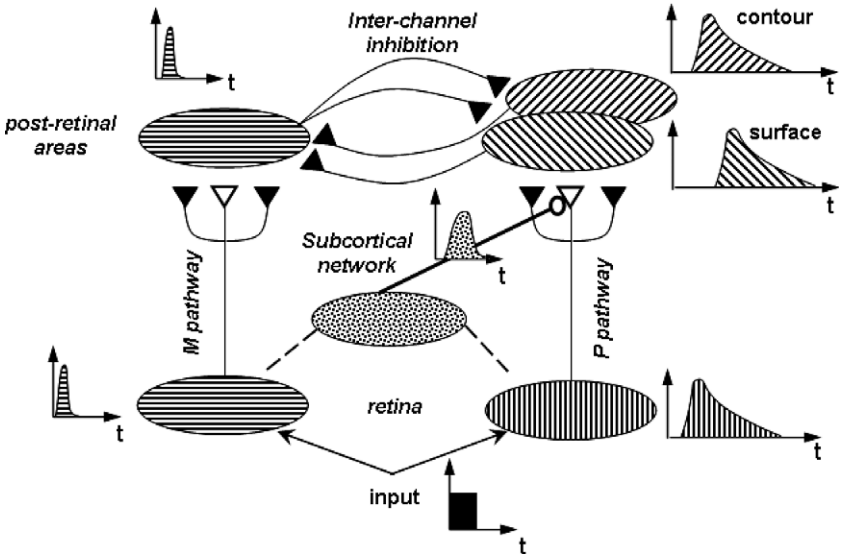

Fig. 4. REtino-COrtical Dynamics (RECOD) model. The input is processed by two retinal ganglion cells populations giving rise to magnocellular (M) and parvocellular (P) pathways. As depicted in the figure, M and P pathways produce short-latency transient and longer-latency sustained responses, respectively. Cortical networks that receive dominant M and P inputs form psychophysically identified transient and sustained channels, respectively. Post-retinal targets of M and P pathways are represented as lumped networks. Here, we unlumped the sustained channel into separate contour and surface networks as shown at the top right of the figure. A subcortical network has been added to account for facilitatory effects in paracontrast. Open and closed triangular symbols depict excitatory and inhibitory connections, respectively. The open circular connection denotes a multiplicative synaptic interaction. For simplicity, only a small subset of connections are shown. For example, to avoid clutter, feedback connections in post-retinal areas are not shown. A complete description of the model is given in Appendix A. Schematic depictions of responses for different cell types are shown next to each sub-network. The response depictions are used in Figs. 5 and 8 to provide an intuitive explanation of model predictions (adapted from Öğmen, 1993).

el) along with experimental data (top panel). In these plots, metacontrast (positive SOAs) and paracontrast (negative SOAs) results are shown together. As discussed in Öğmen et al. (2003), due to computational limitations, simulations of the model involves several simplifications: The simulation is restricted spatially to one dimension only. Within this single dimension, only a region of 3.2 deg extent around the fovea is implemented. As a result, the stimuli used in the simulations are only an approximation of the physical stimuli used in the experiments (one dimensional approximation placed closer to fovea). In our previous study (Öğmen et al., 2003), we found that masking effects in the model were limited to a smaller range of SOAs compared to experimental data. While parametric changes can be made to extend the masking function to longer SOAs, we preferred to keep the parameters same as in our previous study and make comparisons with data while keeping in mind the fact that masking effects in the model span a smaller range of SOAs. Accordingly, the scales in the abscissa for the top and bottom panels in Fig. 6 range from −500 to 400 ms for the data and from −200 to 200 ms for the model. First, consider the results for metacontrast (positive SOAs): Overall, the model captures well the shape of the metacontrast functions. In agreement with data, strongest metacontrast occurs at shorter SOA for the contour network compared to the surface/brightness (20 ms for contour vs. ca. 60 ms for surface) network. The values of SOA where optimal suppression occurs compare well with those observed in the data (10–20 ms for contour vs. 40 ms for surface).

5.2. Paracontrast

The paracontrast results appear to present a more complex picture. We analyze these results in terms of three processes as depicted in Fig. 7. Two of these processes are inhibitory. In our dual-channel model, a suppressive effect is produced by intrachannel center–surround antagonism of sustained (P) neural activity. It is known that the inhibitory surround activation of classical receptive fields is slower by 10–30 ms than activation of the center region (Benardete & Kaplan, 1997; Maffei, Cervetto, & Fiorentini, 1970; Poggio, Baker, Lamarre, & Sanseverino, 1969; Singer & Creutzfeldt, 1970). One would then expect that the surrounding mask has to precede the target by SOAs of −10 to −30 ms to obtain optimal suppression of target-induced excitatory activity. These intrachannel, center–surround inhibitory effects are most likely fast and of a short duration (Connors, Malenka, & Silva, 1988). However, our paracontrast results indicate that an additional inhibitory effect lasts for up to 450 ms. As indicated in the empirical results shown in Fig. 3B, suppression of target visibility can begin when the mask precedes the target by about 450 ms. This effect is explained in our model by a cortical long-lasting intra-channel inhibition (Öğmen et al., 2003). Evidence for both the brief and prolonged inhibition has been found in visual cortex (Berman, Douglas, Martin, & Whitteridge, 1991; Connors et al., 1988; Nelson, 1991). In sum, according to our model the two suppressive effects in paracontrast are: (1) a relatively fast intrachannel inhibition realized in the center–surround antagonism of classical

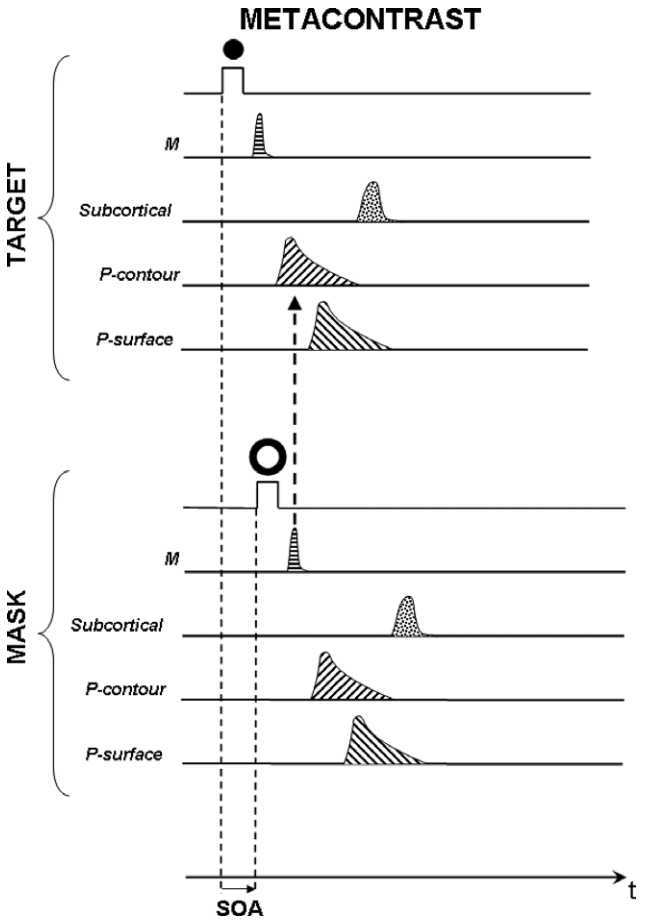

Fig. 5. Schematic diagram of the optimal metacontrast suppression effect of a mask on the contour and brightness visibilities of a prior target stimulus. Dashed vertical arrow indicates inhibition of the target's sustained activity by the mask's transient activity. Same conventions as in Fig. 4 are used in depicting activities. See text for details.

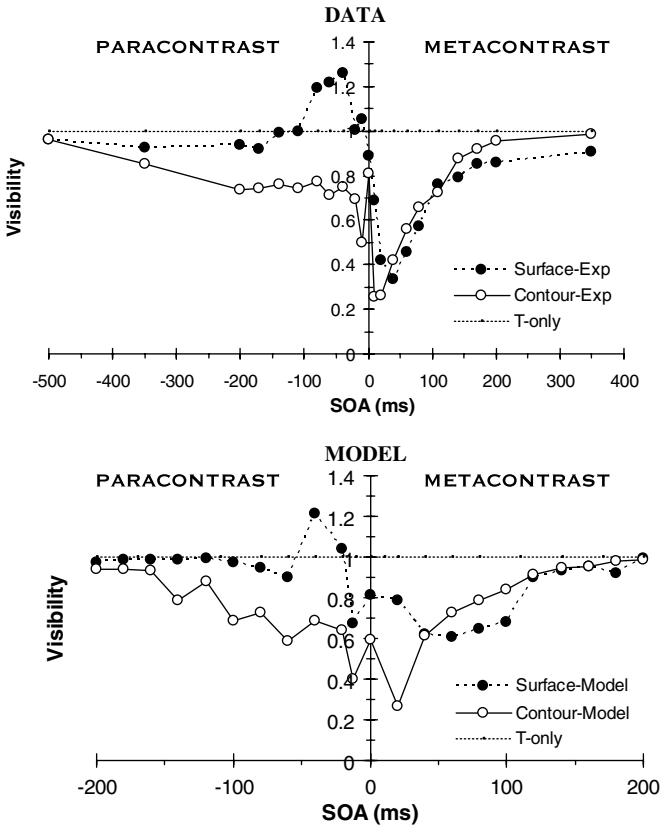

Fig. 6. Combined paracontrast (negative SOAs) and metacontrast (positive SOAs) empirical results are shown in the top panel. Results of model simulations are plotted in the bottom panel. Open and closed symbols represent contour and surface/brightness results, respectively. Results are with respect to "target-only" baseline condition which is normalized to a value of 1. Note that the scales of the abscissa for the top and bottom panels are different. See text for details.

receptive fields, and (2) a slower more prolonged inhibition, associated with other properties of cortical activity.

In addition, our paracontrast results show that a prior mask can have not only suppressive effects on target visibility but also a counteracting facilitating effect. Evidence for facilitatory effects of a prior stimulus on the visibility of a following one has also been reported elsewhere (Bachmann, 1988, 1994; Michaels & Turvey, 1979; Stober et al., 1978). A plausible explanation for the enhancement effect has been proposed by Bachmann (1988, 1994, 1997) in terms of his perceptual retouch (PR) approach. According to PR, a stimulus activates not only afferent pathways that project via the lateral geniculate nucleus to specific visual cortical areas but also pathways projecting to nonspecific activating systems in the subcortical brain-stem and midbrain, which in turn project to the specific cortical areas and enhance activity there (Hartveit, Ramberg, & Heggelund, 1993; Purpura, 1970; Singer, 1977; Singer, Tretter, & Cynader, 1976; Steriade & McCarley, 1990). The response of the subcortical nonspecific system is generally slower by about 50–60 ms than that of the cortical specific systems. Hence, if a stimulus is delayed by about 50 ms

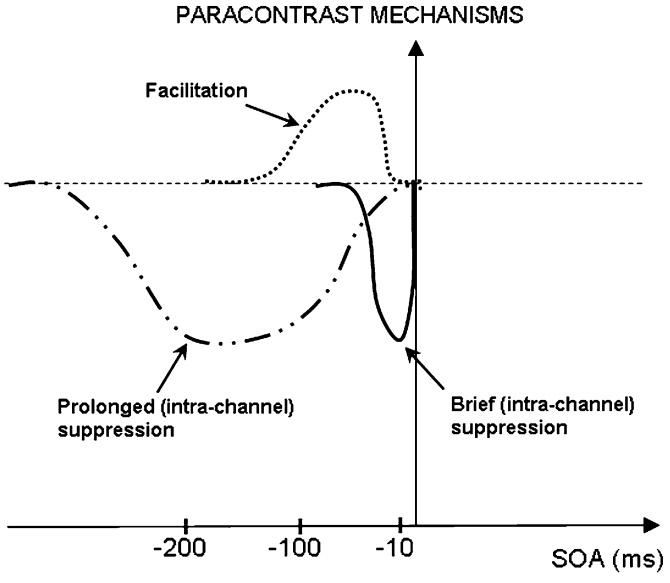

Fig. 7. Schematic diagram of three processes that are proposed to underlie paracontrast effects.

relative to a prior one, the faster specific cortical activity generated by the following stimulus will be maximally enhanced by the slower nonspecific subcortical activation produced by the preceding stimulus. As a result the visibility of the second of two stimuli will be maximally enhanced. To account for the facilitation effect in paracontrast, we introduced to our model an additional network that we tentatively identify as a subcortical network. As shown in Fig. 4, the output of this subcortical network multiplicatively gates the input signals to the surface and contour networks.

Fig. 8 illustrates how a facilitation produced by the slower subcortical system could enhance the visibility of a target's brightness and contour during paracontrast. For instance, as shown, the facilitatory effect on visibility of a target's brightness is maximal when the mask precedes the target at an SOA of a few tens of milliseconds. Although not shown, it is evident from Fig. 8 that the facilitatory effect on visibility of a target's contour is maximal when the mask precedes the target by a slightly larger SOA. Corresponding model simulations are given in Fig. 6. First consider the results for the contour network (Fig. 6, negative SOAs, open symbols). One observes a gradual long-lasting suppression coupled with a strong suppression around SOA = −10 ms. For the surface network (Fig. 6, negative SOAs, filled symbols), the long-lasting suppression is weaker and an enhancement occurs at SOA = −40 ms. This enhancement is followed by a dip at an SOA around −10 ms (the dip is much weaker in the data). The seemingly different morphologies for contour and surface paracontrast functions are obtained in the model by using an identical set of equations. The only difference was the different weightings associated with the inhibitory and facilitatory processes as they interact within surface and contour networks. The long-lasting inhibitory process had a higher weight for the contour network (parameter H^{pi} in the Appendix A, with values 1.5 and 0.2 for contour and surface networks, respectively, as shown in Table A.4) and the multiplicative action of the facilitatory process had a higher gain for the surface network (parameter λ_s in the Appendix A, with values 0.09 and 0.25 for contour and surface networks, respectively, as shown in Table A.4).

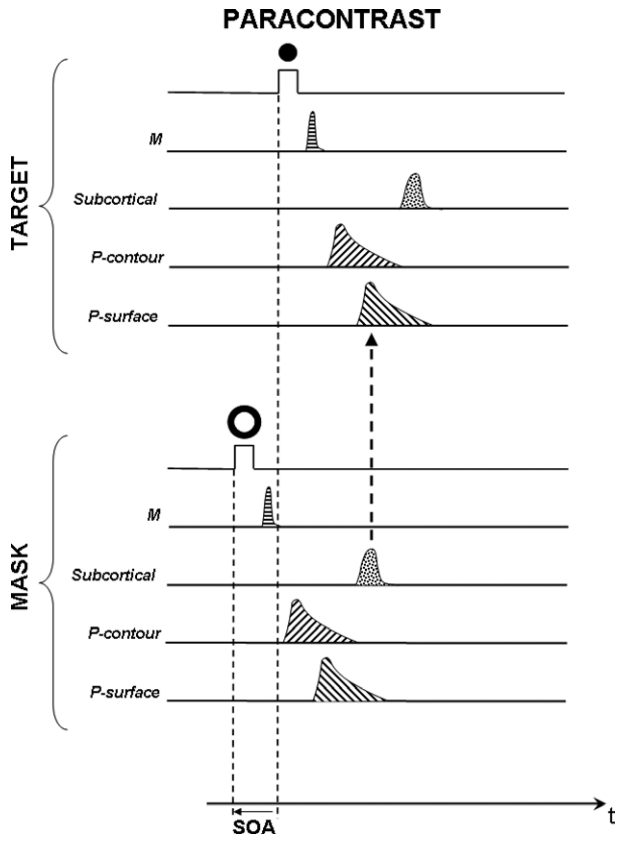

Fig. 8. Schematic diagram of the optimal paracontrast enhancement effect of a mask on the contour and brightness visibilities of a following target stimulus. Dashed vertical arrow indicates facilitation of the target's sustained activity by the mask generated subcortical activity. Same conventions as in Fig. 4 are used in depicting activities. See text for details.

The combined results of our metacontrast and paracontrast experiments indicate (a) that surface features such as brightness and contour features are processed by separate cortical pathways or processes and (b) that the temporal response characteristics of these two processes are distinct, with the contour process having a shorter latency than the brightness process. The former conclusion is supported by theoretical considerations (Grossberg, 1994; Grossberg & Mingolla, 1985) as well as neurophysiological findings (DeYoe & Van Essen, 1988; Lamme et al., 1999; Xiao et al., 2003). The latter conclusion also is consistent with prior theoretical considerations (Arrington, 1994) and psychophysical (Elder & Zucker, 1998) as well as neurophysiological (Lamme et al., 1999) findings. Furthermore, our model simulations suggest that surface and contour networks have similar suppressive and facilitatory processes but these processes interact with different weights within these two networks. It remains to be seen if these conclusions apply also to other surface properties such as color and texture and to contours defined by chromatic and texture differences.

Acknowledgments

This work was supported by NSF grant BCS-0114533 and NIH grant R01-MH49892.

Appendix A. Mathematical description of the RECOD model and simulation methods

A.1. Introduction

The model was identical to that described in Öğmen et al. (2003) with two extensions: (1) unlumping the postretinal network mainly driven by the P-pathway into separate contour and surface networks to account for the differences between these two processes, and (2) incorporation of a subcortical network to account for the facilitatory effects

observed in paracontrast. For sake of completeness, we reproduced from Öğmen et al. (2003) the description of the model and we highlight the aforementioned modifications.

A.2. Fundamental equations of the model and their neurophysiological bases

The first type of equation used in the model has the form of a generic Hodgkin-Huxley equation

$$\frac{dV_m}{dt} = -(E_p + V_m)g_p + (E_d - V_m)g_d - (E_h + V_m)g_h, \tag{A.1}$$

where V_m represents the membrane potential, g_p, g_d, g_h are the conductances for passive, depolarizing, and hyperpolarizing channels, respectively, with E_p, E_d, E_h representing their Nernst potentials. This equation has been used extensively in neural modeling to characterize the dynamics of membrane patches, single cells, as well as networks of cells (rev. Grossberg, 1988; Koch & Segev, 1989). For simplicity, we will assume $E_p = 0$ and use the symbols B, D, and A for E_d, E_h, g_p, respectively to obtain the generic form for "multiplicative" or "shunting" equation (rev. Grossberg, 1988)

$$\frac{dV_m}{dt} = -AV_m + (B - V_m)g_d - (D + V_m)g_h. \tag{A.2}$$

The depolarizing and hyperpolarizing conductances are used to represent the excitatory and inhibitory inputs, respectively.

The second type of equation is a simplified version of Eq. (A.1), called the "additive", "leaky-integrator" model, where the external inputs influence the activity of the cell not through conductance changes but directly as depolarizing and hyperpolarizing currents yielding the form:

$$\frac{dV_m}{dt} = -AV_m + \text{Excitatory Inputs} - \text{Inhibitory Inputs}. \tag{A.3}$$

Mathematical analyses showed that, with appropriate connectivity patterns, shunting networks can automatically adjust their dynamic range to process small and large inputs (rev. Grossberg, 1988). Accordingly, we use shunting equations when we have interactions among a large number of neurons [Eqs. (A.6), (A.8), (A.10) and (A.12)] so that a given neuron can maintain its sensitivity to a small subset of its inputs without running into saturation when a large number of inputs become active. We use the simplified additive equations when the interactions involve few neurons [Eqs. (A.7) and (A.11)]. For simplicity, we also used an additive equation for the newly introduced subcortical network (Eq. (A.9)). The output of this network multiplicatively gates signals which are normalized by a shunting equation (A.10).

Finally, a third type of equation is used to express biochemical reactions of the form

$$S + Z \xrightarrow{\gamma} Y \xrightarrow{\delta} X \xrightarrow{\alpha} S + Z,$$

where a biochemical agent, S, activated by the input, interacts with a transducing agent, Z, (e.g., a neurotransmitter) to produce an "active complex", Y, that carries the signal to the next processing stage. This active complex decays to an inactive state, X, which in turn dissociates back into S and Z. It can be shown that (see Appendix in Sarikaya, Wang, & Öğmen, 1998), when the active state X decays very fast, the dynamics of this system can be written as:

$$\frac{dz}{dt} = \alpha(\beta - z) - \gamma sz, \tag{A.4}$$

with the output given by $y(t) = \frac{\gamma}{\delta}s(t)z(t)$, where s, z, y represent the concentrations of S, Z, and Y, respectively and γ, δ, α denote rates of complex formation, decay to inactive state, and dissociation, respectively. This equation has been used in a variety of neural models, in particular to represent temporal adaptation, or gain control property, occurring for example through synaptic depression (e.g. Abbott, Varela, Sen, & Nelson, 1997; Carpenter & Grossberg, 1981; Gaudiano, 1992; Grossberg, 1972; Öğmen, 1993; Öğmen & Gagné, 1990).

A.3. The retinal network

The retinal network is designed to capture the basic spatio-temporal properties of the retinal output without necessarily incorporating all details of the retinal circuitry. To the extent possible, parameters of the model reflect the physiologically measured parameters of the primate retina.

A.3.1. Retinal cells with sustained activities (parvocellular pathway)

All the equations and the parameters are identical to those used in (Purushothaman, Lacassagne, Bedell, & Öğmen, 2002; Öğmen et al., 2003). The activities of sustained retinal cells are described in three functional stages:

Stage 1: Temporal adaptation (gain control). We use Eq. (A.4) to achieve temporal adaptation (gain control):

$$\frac{1}{\tau}\frac{dz_i}{dt} = \alpha(\beta - z_i) - \gamma(J + I_i)z_i, \tag{A.5}$$

where z_i represents the concentration of a transducing agent at the ith spatial location. J is a baseline input generating a dark current and I_i is the external input (luminance value) at the ith spatial position. This temporal adaptation, or gain control, stage causes the neural activity to decay to a plateau level after an initial peak response to a sustained input, as observed in sustained retinal ganglion cell responses. The parameter τ adjusts the time-constant of the decaying response. The parameter values of this equation are given in Table A.1.

Stage 2: Spatial center–surround organization. Signals from the first stage are convolved by the kernels G_k^{se} and G_k^{si} which represent the excitatory-center and the inhibitory-surround of the receptive field. The kernels are Gaussian

Table A.1
Choice of parameter values for Eq. (A.5)

Parameter	Value
α	0.40
β	16.0
γ	0.13
J	12.0
τ	0.0035

functions of the form $G_k^{se} = \mathrm{Amp}_{se} e^{-\frac{k^2}{sd_{se}^2}}$ and the parameters Amp_{se} and sd_{se} were selected according to the receptor spacing at the fovea (Coletta & Williams, 1987; Dacey, 1993) and the physiologically measured receptive field characteristics at the corresponding region of the primate retina (Croner & Kaplan, 1995). For simplicity, only the on-center, off-surround-cells were considered. The membrane potential of the ith sustained cell, w_i, is described by

$$\frac{1}{\tau}\frac{dw_i}{dt} = -A_s w_i + (B_s - w_i)\sum_{j=i-n_s}^{i+n_s} G_{j-i}^{se}\Psi(J_s + I_j)z_j - (D_s + w_i)\sum_{j=i-n_s}^{i+n_s} G_{j-i}^{si}\Psi(J_s + I_j)z_j, \quad (A.6)$$

where the center and surround convolution sums provide the excitatory and the inhibitory inputs to a shunting equation (compare Eqs. (A.2) and (A.6)). The input signal is processed by a second order polynomial, $\Psi(.)$, whose coefficients were determined by fitting the contrast response of the model neurons to the physiological data from Kaplan and Shapley (1986) (see Appendix A.1. and Fig. 6 in Purushothaman et al., 2002).

Stage 3: Quadratic-nonlinearity-with-threshold and persistence. The "membrane potential" of the ith cell is transformed into an output signal (e.g., spike frequency) through a quadratic nonlinearity with threshold, $\lambda([w_i - \Gamma_s]^+)^2$, where $[a]^+$ denotes the threshold, or half-wave rectification, function (i.e. $[a]^+ = a$ if $a > 0$ and $[a]^+ = 0$, otherwise). Parameters λ, Γ_s represent the gain and the threshold level of this function, respectively. The thresholded signal provides the input to the additive equation

$$\frac{dv_i}{dt} = \sigma(-v_i + \lambda([w_i - \Gamma_s]^+)^2), \quad (A.7)$$

whose parameter σ determines the overall temporal persistence of the signal in the parvocellular pathway.

A.3.2. Retinal cells with transient activities (magnocellular pathway)

The spatial receptive-field profile of transient cells is modeled using a Gaussian kernel whose parameters (see Table A.2) reflect physiologically measured receptive field characteristics of the transient cells in the primate retina (Croner & Kaplan, 1995). The surround of the receptive-field integrates inputs with low sensitivity but over a relatively large retinal area. The relatively small one-dimensional stimuli used in our simulations do not produce any appreciable surround response. Therefore, we used only the center of the receptive field in a shunting equation given by:

Table A.2
Choice of parameter values for retinal network equations

Parameter	Value
A_s	2.0
B_s	250.0
D_s	10.0
J_s	6.0
G^{se}: Amp	1.0
G^{se}: sd	(0.03 * 60.0 * 60.0)/23.0
G^{si}: Amp	0.0135
G^{si}: sd	(0.18 * 60.0 * 60.0)/23.0
σ	0.10
λ	0.00125
Γ_s	230.877
n_s	28.0
n_t	40.0
A_t	2.0
B_t	600.0
δ	1.0
G^{tse}: Amp	0.00743
G^{tse}: sd	(0.1 * 60 * 60)/23.0

$$\frac{dy_i}{dt} = -A_t y_i + (B_t - y_i)\sum_{j=i-n_t}^{i+n_t} G_{j-i}^{tse}\{I_j(t) - I_j(t-\delta)\}. \quad (A.8)$$

A delayed version of the input (delay $= \delta$) is subtracted from the input to generate transient responses (backward-difference formula). The parameter values of the retinal network equations are listed in Table A.2.

A.4. The subcortical network

This network has been added to the description in Öğmen et al. (2003) to account for the facilitatory effect observed in paracontrast. The main requirement for this network is a relatively slow activity that gates inputs to the cortical surface network. However, for definiteness, following Bachmann's (1994) approach we identified this network as a sub-cortical network. For simplicity we provide an input to this network directly from retinal cells with transient activities. The activity of the ith cell, s_i, in the subcortical network is governed by the additive equation

$$\frac{ds_i}{dt} = \sigma_s(-s_i + \sum_{j=i-\Delta}^{i+\Delta} y_j). \quad (A.9)$$

Parameters σ_s, Δ represent the time constant of activity dynamics and the spatial spread of the summation, respectively. The values of these parameters are listed in Table A.3.

A.5. The post-retinal network

Because of its staggering complexity, a detailed model of the post-retinal network (lateral geniculate nucleus (LGN)

Table A.3
Choice of parameter values for the subcortical network equation

Parameter	Value
σ_s	0.00035
Δ	60

and visual cortical areas) would be computationally intractable. Our approach is to use a lumped network that is tailored according to the requirements of the simulation. For example, Öğmen et al.'s (2003) study did not investigate separately surface and contour perception and a single lumped post-retinal network was used to represent all cortical targets of the P-pathway. Here, we split this lumped network into two networks, one representing cells processing contour properties and a second one representing cells processing surface properties. For simplicity, we used identical networks and the only differences between the two networks were the values of three parameters as discussed below.

A.5.1. Post-retinal cells mainly driven by the parvo-cellular pathway ('post-retinal sustained cells''). The contour network

The activity of the ith cell, p_i, is given by the shunting equation

$$\frac{1}{\tau}\frac{dp_i}{dt} = -A_p p_i + (B_p - p_i)\{\Phi(p_i) + (2 + \lambda_s[s_i(t-\eta-\kappa_s)]^+) \times v_i(t-\eta)\} - p_i\left\{\sum_{j=i-n_{pf};j\neq i}^{i+n_{pf}} \Phi(p_j) + \sum_{j=i-n_p}^{i+n_p} H^{pi}_{j-i} v_j(t-\eta-\kappa_p) + \sum_{j=i-n_p}^{i+n_p} Q^{mp}_{j-i} m_j\right\}, \quad (A.10)$$

where the excitation consists of the afferent parvocellular signal and a feedback signal. The inhibitory signal consists of feedback, feed-forward, inter-channel terms. Excitatory and inhibitory recurrent (feedback, re-entrant) signals are carried out through the nonlinear function $\Phi(a) = 10a\{(a+1)^2 - 1\}$, if $a < 0.05$ and $\Phi(a) = a(a + 0.975)$, otherwise. This function and its parameters were chosen to achieve sharpening of boundary signals for dynamic inputs (Öğmen, 1993). The inhibitory kernels, H^{pi}_k and Q^{mp}_k, determine the spatial spread of intra- and inter-channel inhibition, respectively. Parameter η represents the relative delay between the parvocellular and magnocellular signals. Parameter κ_p reflects the relative delay of the inter-channel inhibitory signal with respect to the excitatory signal. Compared to the equivalent equation in Öğmen et al. (2003), this equation has been modified to include a signal from the subcortical network, $([s_i(t-\eta-\kappa_s)]^+)$, which modulates the excitatory parvocellular signal multiplicatively. Parameter λ_s determines the gain of this multiplicative action. When it is zero, the equation becomes identical to that in Öğmen et al. (2003). Parameter κ_s represents the relative delay between the parvocellular and sub-cortical network signals.

A.5.2. Post-retinal cells mainly driven by the parvo-cellular pathway ('post-retinal sustained cells''). The surface network

These cells obey an equation identical to the contour network cell Eq. (A.10). The only differences between these networks are the values of three parameters as shown in Table A.4. Through parameter η, the surface network has a longer latency than the contour network; through parameter H^{pi}, the surface network has weaker magnitude for the long-lasting intra-channel inhibition, and finally through parameter λ_s the surface network has a stronger gain for the multiplicative facilitatory action of the subcortical network.

A.5.3. Post-retinal inhibitory inter-neurons

The post-retinal inhibitory inter-neurons carry the inhibition from sustained cortical cells to transient cortical cells via the additive equation:

$$\frac{dq_i}{dt} = -A_q q_i + B_q p_i, \quad (A.11)$$

where q_i is the activity of the ith post-retinal inhibitory inter-neuron.

A.5.4. Post-retinal cells mainly driven by the magno-cellular pathway (''post-retinal transient cells'')

The post-retinal transient cells receive excitatory and inhibitory inputs from the magnocellular pathway and a post-retinal sustained-on-transient inhibition via the kernel Q^{pm}_k yielding the shunting equation:

Table A.4
Choice of parameter values for post-retinal network equations

Parameter	Value
A_p	1.0
B_p	1.0
η: Contour	2.0
η: Surface	7.0
λ_s: Contour	0.09
λ_s: Surface	0.25
n_{pf}	24
n_p	120
κ_s	10.0
κ_p	9.0
H^{pi}: Amp Contour	1.5
H^{pi}: Amp Surface	0.2
H^{pi}: sd	100.0
Q^{mp}: Amp	5.0
Q^{mp}: sd	100.0
A_q	1.0
B_q	10.0
A_m	10.0
B_m	1.0
κ_m	10.0
H^{mi}: Amp	7.0
H^{mi}: sd	56.0
Q^{pm}: Amp	300.0
Q^{pm}: sd	80.0

$$\frac{dm_i}{dt} = -A_m m_i + (B_m - m_i)2[y_i(t)]^{++} - m_i\{\sum_{j=i-n_p}^{i+n_p} H^{mi}_{j-i}[y_j(t-\kappa_m)]^{++} + \sum_{j=i-n_p}^{i+n_p} Q^{pm}_{j-i} q_j\}, \quad (A.12)$$

where m_i is the activity of the ith post-retinal transient cell. The function $[.]^{++}$ denotes full-wave rectification that generates the "on–off" response characteristics of transient cells. Parameter κ_m reflects the relative delay of the intrachannel inhibitory signal with respect to the excitatory signal. The parameter values of the post retinal network equations are listed in Table A.4.

A.6. Simulation methods

The system of ordinary differential equations was solved numerically with the CVODE package. This package uses variable-coefficient forms of the Adams and backward differentiation formula methods (Cohen & Hindmarsh, 1994). The programs were written in C and were run on SUN workstations. Numerical solutions of large systems of ODEs can be very time consuming. The model was simplified to keep the simulations within reasonable bounds. The model contains only one spatial dimension, which was sampled at 500 positions (i.e. $1 \leqslant i \leqslant 500$). At the foveal inter-receptor spacing of 23 s, this results in a region of 3.2 deg extent. To simplify the computations, the convolution sums were carried out with a fixed extent given by $n_s = 28$, $n_t = 40$, and $n_p = 120$. The target covered 19 spatial positions (at 23 s spacing, this corresponds to a size of 7 min). It was flanked on both sides by masks of the same size. Center-to-center separation between the target and the masks was 30 spatial positions, corresponding to an edge-to-edge separation of 4 min. The magnitudes of the target and the mask inputs were 1 (arbitrary) unit above a background of 1 unit. The durations of the target and mask stimuli were 2.5 simulation-time units. In Öğmen et al. (2003), one simulation-time unit corresponded to 8 ms real-time. To bring the dips to the range observed in the empirical data, here we used a calibration where 1 simulation-time unit corresponded to 4 ms real-time. With this calibration, stimuli durations were 2.5×4 ms $= 10$ ms each. Target visibility was computed as the space-time-integrated activity of the post-retinal sustained cells responding to the target (computed at the 19 positions occupied by the target stimulus). The integrated space-time activity obtained from the surface network provided "perceived brightness". The integrated space-time activity obtained from the contour network provided a measure of contour visibility. In order to compare these to experimental data, we used a single scaling procedure as follows: First we divided space-time-integrated activities obtained when the target is presented with the mask ($T_{\text{with-mask}}$) by the space-time-integrated activities obtained when the target is presented without the mask ($T_{\text{without-mask}}$). This ratio, $T_{\text{with-mask}}/T_{\text{without-mask}}$, provides a relative measure of target visibility with respect to the baseline where the target is presented in isolation. To scale this ratio, we subtracted the baseline value 1, multiplied by a scaling factor, and added back the baseline value. We used the value 1.8 as scaling factor giving the overall scaling equation:

$$T_{\text{scaled}} = 1.8\left(\frac{T_{\text{with-mask}}}{T_{\text{without-mask}}} - 1\right) + 1. \quad (A.13)$$

A.7. Parameter values

A fixed set of parameters was used in all simulations. These parameters were identical to those used in Öğmen et al. (2003) with the aforementioned exceptions. The values of the parameters are given in Tables A.1–A.3.

References

Abbott, L. F., Varela, K., Sen, K., & Nelson, S. B. (1997). Synaptic depression and cortical gain control. *Science, 275*, 220–223.

Alpern, M. (1953). Metacontrast. *Journal of the Optical Society of America, 43*, 648–657.

Arrington, K. F. (1994). The temporal dynamics of brightness filling-in. *Vision Research, 34*, 3371–3387.

Bachmann, T. (1988). Time course of the subjective contrast enhancement for a second stimulus in successively paired above-threshold transient forms: Perceptual retouch instead of forward masking. *Vision Research, 28*, 1255–1261.

Bachmann, T. (1994). *Psychophysiology of visual masking: The fine structure of conscious experience*. ommack, NY: Nova Science Publishers.

Bachmann, T. (1997). Visibility of brief images: the dual-process approach. *Consciousness and Cognition, 6*, 491–518.

Benardete, E. A., & Kaplan, E. (1997). The receptive field of the primate P retinal ganglion cell, I: Linear dynamics. *Visual Neuroscience, 14*, 169–185.

Berman, N. J., Douglas, R. J., Martin, K. A., & Whitteridge, D. (1991). Mechanisms of inhibition in cat visual cortex. *Journal of Physiology, 440*, 697–722.

Bernstein, I., Amundson, V. E., & Schurman, D. L. (1973). Metacontrast inferred from reaction time and verbal report: Replications and comments on the Fehrer-Biederman experiment. *Journal of Experimental Psychology, 100*, 195–201.

Bernstein, I. H., Fisicaro, S. A., & Fox, J. A. (1976). Metacontrast suppression and criterion content: A discriminant function analysis. *Perception & Psychophysics, 20*, 198–204.

Breitmeyer, B. G., & Ganz, L. (1976). Implications of sustained and transient channels for theories of visual pattern masking, saccadic suppression and information processing. *Psychological Review, 83*, 1–36.

Breitmeyer, B. G., Love, R., & Wepman, B. (1974). Contour masking during stroboscopic motion and metacontrast. *Vision Research, 14*, 1451–1456.

Breitmeyer, B. G., & Ogmen, H. (2000). Recent models and findings in visual backward masking: a comparison, review, and update. *Perception & Psychophysics, 62*, 1572–1595.

Carpenter, G. A., & Grossberg, S. (1981). Adaptation and transmitter gating in vertebrate photoreceptors. *Journal of Theoretical Neurobiology, 1*, 1–42.

Cavonius, C. R., & Reeves, A. J. (1983). The interpretation of metacontrast and contrast-flash spectral sensitivity functions. In J. D. Mollon & L. T. Sharpe (Eds.), *Color vision: Physiology and psychophysics* (pp. 471–478). London: Academic Press.

Cohen, S. D., & Hindmarsh, A. C. (1994). *CVODE User Guide*. UCRL-MA-118618.

Coletta, N. J., & Williams, D. R. (1987). Psychophysical estimate of extrafoveal cone spacing. *Journal of The Optical Society of America A, 4*, 1503–1513.

Connors, B. W., Malenka, R. C., & Silva, L. R. (1988). Two inhibitory postsynaptic potentials, and GABAA and GABAB receptor-mediated responses in neocortex of rat and cat. *Journal of Physiology, 406*, 443–468.

Croner, L. J., & Kaplan, E. (1995). Receptive fields of P and M ganglion cells across the primate retina. *Vision Research, 35*, 7–24.

Dacey, D. M. (1993). The mosaic of midget ganglion cells in the human retina. *Journal of Neuroscience, 13*, 5334–5355.

DeYoe, E. A., & Van Essen, D. C. (1988). Concurrent processing streams in monkey visual cortex. *Trends in Neuroscience, 11*, 219–226.

Elder, J. H., & Zucker, S. W. (1998). Evidence for boundary-specific grouping. *Vision Research, 38*, 143–152.

Enns, J. T., & Di Lollo, V. (1997). Object substitution: A new form of masking in unattended visual locations. *Psychological Science, 8*, 135–139.

Fehrer, E., & Biederman, I. (1962). A comparison of reaction and verbal report in detection of masked stimuli. *Journal of Experimental Psychology, 64*, 126–130.

Fehrer, E., & Raab, D. (1962). Reaction time to stimuli masked by metacontrast. *Journal of Experimental Psychology, 63*, 143–147.

Foster, D. H., & Mason, R. J. (1977). Interaction between rod and cone systems in dichoptic visual masking. *Neuroscience Letters, 4*, 39–42.

Francis, G. (1996a). Cortical dynamics of visual persistence and temporal integration. *Perception & Psychophysics, 58*, 1203–1212.

Francis, G. (1996b). Cortical dynamics of lateral inhibition: visual persistence and ISI. *Perception & Psychophysics, 58*, 1103–1109.

Francis, G. (1997). Cortical dynamics of lateral inhibition: Metacontrast masking. *Psychological Review, 104*, 572–594.

Gaudiano, P. (1992). A unified neural network of spatio-temporal processing in X and Y retinal ganglion cells. II: Temporal adaptation and simulation of experimental data. *Biological Cybernetics, 67*, 23–34.

Grossberg, S. (1972). A neural theory of punishment and avoidance, II: Quantitative theory. *Mathematical Biosciences, 15*, 253–285.

Grossberg, S. (1988). Nonlinear neural networks: Principles, mechanisms, and architectures. *Neural Networks, 1*, 17–61.

Grossberg, S. (1994). 3-D vision and figure-ground separation by visual cortex. *Perception & Psychophysics, 55*, 48–120.

Grossberg, S., & Mingolla, E. (1985). Neural dynamics of form perception: Boundary completion, illusory figures, and neon color spreading. *Psychological Review, 92*, 173–211.

Harrison, K., & Fox, R. (1966). Replication of reaction time to stimuli masked by metacontrast. *Journal of Experimental Psychology, 71*, 162–163.

Hartveit, E., Ramberg, S. I., & Heggelund, P. (1993). Brainstem modulation of spatial receptive field properties of single cells in the dorsal lateral geniculate nucleus of the cat. *Journal of Neurophysiology, 70*, 1644–1655.

Hernandez, L. L., & Lefton, L. A. (1977). Metacontrast as measured under signal detection model. *Perception, 6*, 696–702.

Hofer, D., Walder, F., & Groner, M. (1989). Metakontrast: ein berühmtes, aber schwer messbares Phänomen. *Schweizerische Zeitschrift für Psychologie, 48*, 219–232.

Kahneman, D. (1968). Method, findings, and theory in studies of visual masking. *Psychological Bulletin, 70*, 404–425.

Kaitz, M., Monitz, J., & Nesher, R. (1985). Electrophysiological correlates of visual masking. *International Journal of Neuroscience, 28*, 261–268.

Kaplan, E., & Shapley, R. M. (1986). The primate retina contains two types of ganglion cells, with high and low contrast sensitivity. *Proceedings of the National Academy of Sciences USA, 83*, 2755–2757.

Koch, C., & Segev, I. (1989). *Methods in neuronal modeling*. Cambridge, MA: MIT Press..

Kolers, P., & Rosner, B. S. (1960). On visual masking (metacontrast): Dichoptic observations. *American Journal of Psychology, 73*, 2–21.

Lamme, V. A. F., Rodriguez-Rodriguez, V., & Spekreijse, H. (1999). Separate processing dynamics for texture elements, boundaries and surgfaces in primary visual cortex of the macaque monkey. *Cerebral Cortex, 9*, 406–413.

Lee, T., Mumford, D., & Schiller, P. (1995). Neuronal correlates of boundary and medial axis representations in primate visual cortex. *Journal of Investigative Ophthalmology and Visual Science, 36*, 477.

Maffei, L., Cervetto, L., & Fiorentini, A. (1970). Transfer characteristics of excitation and inhibition in cat retinal ganglion cells. *Journal of Neurophysiology, 33*, 276–284.

Michaels, C. F., & Turvey, M. T. (1979). Central sources of visual masking: Indexing structures supporting seeing at a single, brief glance. *Psychological Research, 41*, 1–61.

Nelson, S. B. (1991). Temporal interactions in the cat visual system. I. Orientation-selective suppression in the visual cortex. *Journal of Neuroscience, 11*, 344–356.

Öğmen, H. (1993). A neural theory of retino-cortical dynamics. *Neural Networks, 6*, 245–273.

Öğmen, H., Breitmeyer, B. G., & Melvin, R. (2003). The what and where in visual masking. *Vision Research, 43*, 1337–1350.

Öğmen, H., & Gagné, S. (1990). Neural models for sustained and on–off units of insect lamina. *Biological Cybernetics, 63*, 51–60.

Paradiso, M. A., & Nakayama, K. (1991). Brightness perception and filling-in. *Vision Research, 31*, 1221–1236.

Petry, S. (1978). Perceptual changes during metacontrast. *Vision Research, 18*, 1337–1341.

Poggio, G. B., Baker, F. H., Lamarre, Y., & Sanseverino, E. R. (1969). Afferent inhibition at input to visual cortex of the cat. *Journal of Neurophysiology, 32*, 916–929.

Purushothaman, G., Lacassagne, D., Bedell, H. E., & Öğmen, H. (2002). Effect of exposure duration, contrast and base blur on coding and discrimination of edges. *Spatial Vision, 15*, 341–376.

Purpura, D. P. (1970). Operations and processes in thalamic and synaptically related neural subsystems. In F. O. Schmitt (Ed.), *The neurosciences, Second study program* (pp. 458–470). New York: The Rockefeller University Press.

Sarikaya, M., Wang, W., & Öğmen, H. (1998). Neural network model of on-off units in the fly visual system: simulations of dynamic behavior. *Biological Cybernetics, 78*, 399–412.

Singer, W. (1977). Control of thalamic transmission by corticofugal and ascending reticular pathways in the visual system. *Physiological Reviews, 57*, 386–420.

Singer, W., & Creutzfeldt, O. D. (1970). Reciprocal lateral inhibition of on- and off-center neurones in the lateral geniculate body of the cat. *Experimental Brain Research, 10*, 311–330.

Singer, W., Tretter, F., & Cynader, M. (1976). The effect of reticular stimulation on spontaneous and evoked activity in the cat visual cortex. *Brain Research, 102*, 71–90.

Steriade, M., & McCarley, R. W. (1990). *Brainstem control of wakefulness and sleep*. New York: Plenum Press.

Stober, R. S., Brussel, E. M., & Komoda, M. K. (1978). Differential effects pf metacontrast on target brightness and clarity. *Bulletin of the Psychonomic Society, 12*, 433–436.

Stoper, A. E., & Mansfield, J. G. (1978). Metacontrast and paracontrast suppression of a contourless area. *Vision Research, 18*, 1669–1674.

Tata, M. S. (2002). Attend to it now or lose it forever: Selective attention, metacontrast masking, and object substitution. *Perception & Psychophysics, 64*, 1028–1038.

Ventura, J. (1980). Foveal metacontrast: I. Criterion content and practice effects. *Journal of Experimental Psychology: Human Perception and Performance, 6*, 473–485.

Vorberg, D., Mattler, U., Heinecke, A., Schmidt, T., & Schwarzbach, J. (2003). Different time course for visual perception and action priming. *Proceedings of the National Academy of Sciences USA, 100*, 6275–6280.

Vorberg, D., Mattler, U., Heinecke, A., Schmidt, T., & Schwarzbach, J. (2004). Invariant time course of priming with and without awareness. In C. Kaernbach, E. Schröger, & H. Müller (Eds.), *Psychophysics beyond sensation. Laws and invariants of human cognition* (pp. 271–288). Mahwah, NJ: Erlbaum.

Weisstein, N. (1972). Metacontrast. In D. Jameson & L. M. Hurvich (Eds.), *Handbook of sensory physiology, Vol. 7/4, Visual psychophysics* (pp. 233–272). New York: Springer.

Xiao, Y., Wang, Y., & Felleman, D. J. (2003). A spatially organized representation of colour in macaque cortical area V2. *Nature, 421*, 535–539.